ferred into the semiconductor in a series of dry etching steps.[2] This layer was subsequently undercut forming a suspended membrane. The laser cavity is formed by leaving 19 holes out of the photonic crystal lattice. The laser cavity is about 2.5 μm in diameter and the entire structure is less than 8 μm across. Figure 1 shows an electron micrograph of one of the laser cavities used in this study. Arrays of these laser cavities were defined in which the lattice constant varied in increments of 2 nm between adjacent devices. The array contained 31 lasers with lattice constants varying between 490 nm and 550 nm. Figure 2 shows a cross-sectional view of a row of laser cavities with a V-shaped undercut region. The lasers are in the top 224 nm thick membrane, which contains 4 strained InGaAsP quantum wells.

The lasers were optically pumped at room temperature by a VCSEL emitting at 852 nm.[3] The pulse width was fixed at 20 ns with a 1% duty cycle. Lasing spectra from 9 adjacent lasers in the array are shown below in figure 3. The lattice constants in this set of devices varied between 498 nm and 514 nm in 2 nm steps. The lasing wavelength accordingly varied from 1617.0 nm to 1654.5 nm. The wavelength step between adjacent devices varies between 4 nm and 6 nm in this set of lasers. The intensities of these devices are of the same order. Variations shown in the figure are due to variations in signal collection caused by variations in optical alignment. A more complete plot of the lasing wavelengths of all 31 lasers in the array is shown below in figure 4. In this plot the lattice constant varies between 490 nm and 55 nm while the lasing wavelength varies over a range of about 80 nm. The figure shows that as the resonant cavity wavelength tunes past the gain region the lasing mode hops to a shorter wavelength, which also tunes with lattice constant.

In conclusion, we have demonstrated lithographic tuning of photonic crystal lasers with wavelength separations as small as 4 nm between adjacent devices. This technology could be a promising candidate for future WDM systems.

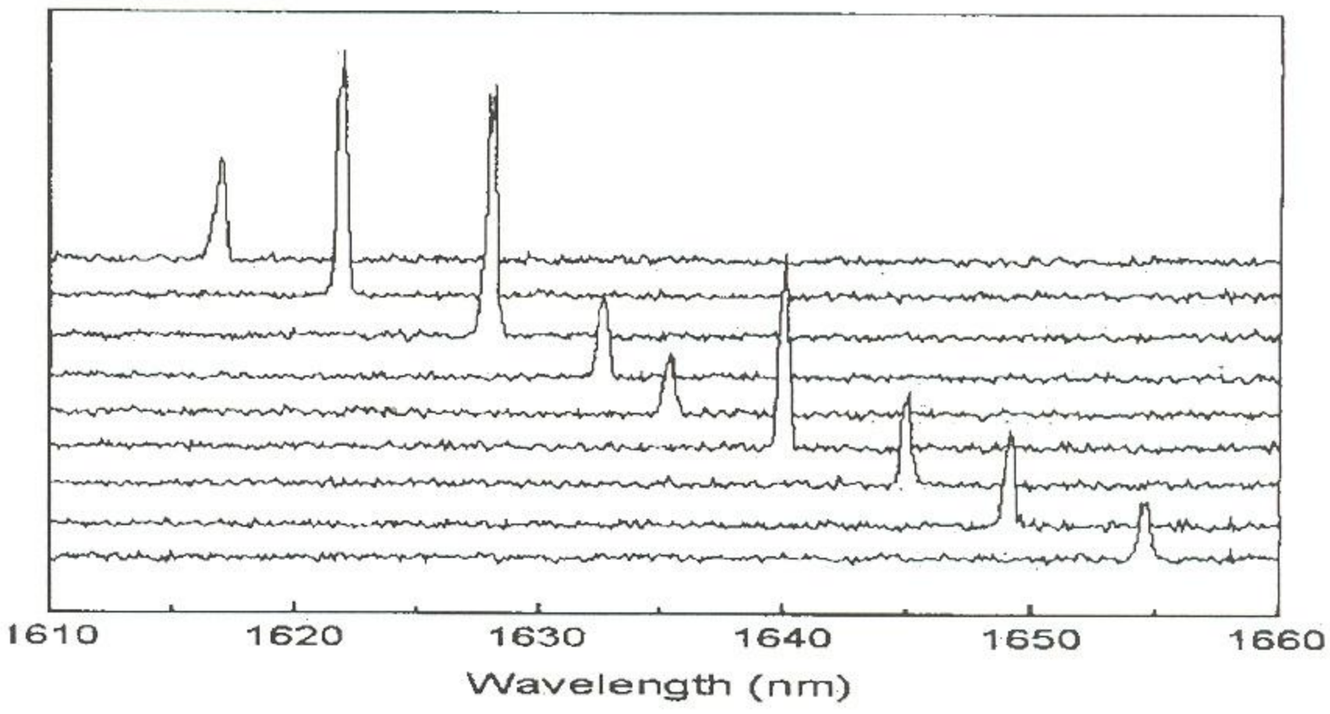

TuW4 **Fig. 3.** Spectra from 9 adjacent lasers in the array.

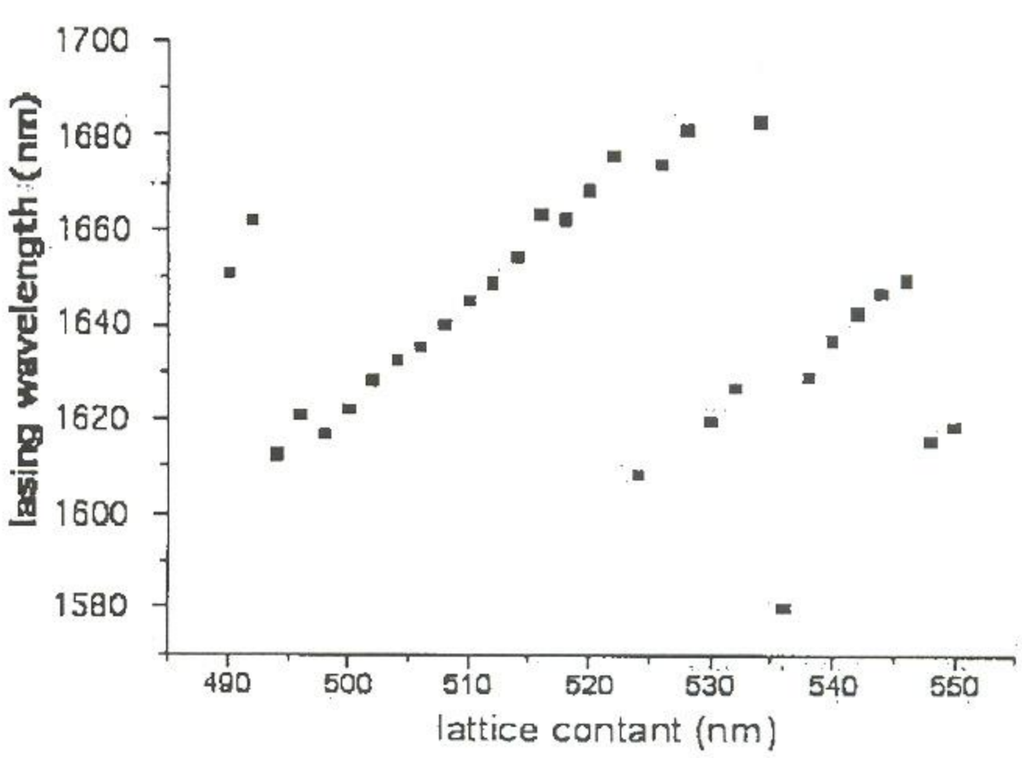

TuW4 **Fig. 4.** Lasing wavelength of all 31 elements in the array as a function of their lattice constant.

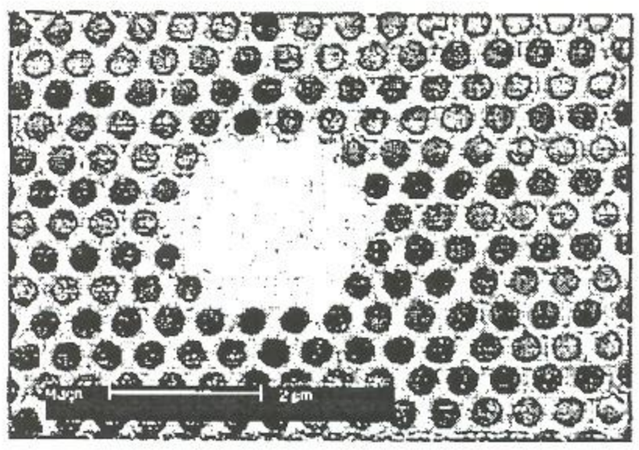

TuW4 **Fig. 1.** Electron micrograph of the top view of a laser cavity.

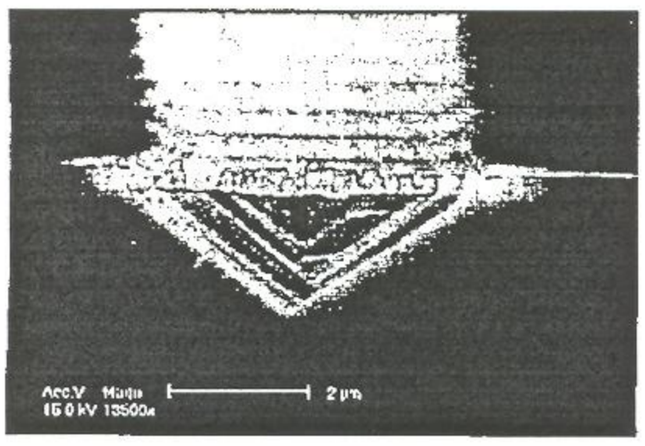

TuW4 **Fig. 2.** Micrograph showing a cross-sectional view of a row of laser cavities.

1. O. Painter, A. Husain, A. Scherer, P.T. Lee, I. Kim, J.D. O'Brien, P.D. Dapkus, "Lithographic Tuning of a Two-Dimensional Photonic Crystal Laser Array", IEEE Phot. Tech. Lett., 12, 1126 (2000).
2. P.T. Lee, J.R. Cao, C.W. Kim, W.J. Kim, S.J. Choi, Z.J. Wei, J.D. O'Brien, P.D. Dapkus, "Room temperature photonic crystal defect lasers", submitted to IEEE J. Quantum Electron., (2001).
3. P.T. Lee, J.R. Cao, S.J. Choi, Z.J. Wei, J.D. O'Brien, P.D. Dapkus, "Room temperature operation of VCSEL-pumped Photonic Crystal Lasers", submitted to IEEE Phot. Tech. Lett. (2001).

TuW5 **5:30 pm**

10 Gb/s optically preamplified receiver using a vertical-cavity amplifying optical filter

E.S. Björlin, J. Geske, and J.E. Bowers, *University of California at Santa Barbara, ECE Dept., Santa Barbara, CA 93106, USA, Email: bjorlin@opto.ucsb.edu*

1. Introduction

Today's high capacity optical communication networks require highly sensitive, low cost receivers running at very high bit rates. An attractive way to achieve high sensitivity at high bit rates is by optical preamplification. This has been demonstrated using both erbium doped fiber amplifiers (EDFAs)[1] and semiconductor optical amplifiers (SOAs).[2] However, EDFAs are limited to operation around 1.55 μm and conventional in-plane SOAs are typically sensitive to the polarization of the signal light. An alternative approach is vertical-cavity semiconductor optical amplifiers (VCSOAs). The vertical-cavity geometry supports a circular-symmetrical mode, which results in high coupling efficiency to optical fiber as well as insensitivity to the polarization of the signal light. Good coupling efficiency is beneficial

for obtaining a low noise figure. Furthermore, the vertical-cavity structure is compatible with low-cost manufacturing and testing techniques as well as integration in high-density 2-dimensional array architectures.

The gain per pass in a VCSOA is small; feedback is used to provide sufficient signal gain. The optical bandwidth is therefore limited to the linewidth of the Fabry-Perot mode, which allows the VCSOA to function as an amplifying filter.[3] This makes VCSOAs ideal as preamplifiers in wavelength division multiplexed (WDM) systems where channel selection is required. The VCSOA bandwidth is determined by the mirror reflectivity, the gain per pass and the length of the cavity. The bandwidth can therefore be tailored to suit different applications or different channel spacing in WDM systems. The narrow filter bandwidth typically needed in such systems is easily obtained using high reflectivity distributed Bragg reflectors (DBRs).

2. Device structure

The VCSOA used in this experiment is a planar, gain guided structure optimized for reflection mode operation. It was optically pumped through the bottom DBR and GaAs substrate using a JDS Uniphase 980-nm laser diode. The spot size of the pump beam (about 8 μm) defines the lateral dimensions of the active region of the VCSOA. The device structure consists of a multiple quantum well (MQW) InGaAsP/InP active region wafer bonded to two GaAs/Al(Ga)As distributed Bragg reflectors (DBRs). Details about wafer bonding can be found in Black et al.[4] The active region has 21 compressively strained $InAs_{0.5}P_{0.5}$ QWs surrounded by strain compensating $In_{0.8}Ga_{0.2}P$ barriers. The QWs are placed in 3 groups of seven wells each, over the three central standing wave peaks in the 5/2λ-cavity. The operation wavelength is 1.3 μm. The bottom and top DBRs have 26 and 13.5 periods, respectively. The calculated mirror reflectivities are 0.999 (bottom) and 0.955 (top). A VCSOA operating at 1.55 μm can be fabricated using the same technology.

A schematic of the experimental setup is shown in Figure 1. The 980 nm pump beam was focused onto the backside of the chip using free-space optics. A 1.3-μm external-cavity tunable laser was used as a signal source. The signal was coupled into, and out from, the VCSOA through the top DBR. A focusing lens was used to inject and collect the signal. The input and output signal were separated using an optical circulator. An optical spectrum analyzer was used to monitor the output spectrum for gain bandwidth measurements. For the transmission measurements, a 10 Gb/s pattern generator driving a $LiNbO_3$ Mach-Zehnder modulator was used to modulate the signal. The optically preamplified receiver (dashed box) consists of the VCSOA, a Nortel PP-10G PIN receiver, a DC block, and an SHF broadband amplifier. The electrical signal from the SHF amplifier was fed to a bit error rate tester. No optical filter was used between the VCSOA and the PIN detector.

3. Experiment

The signal gain and optical bandwidth of the VCSOA were measured in order to determine the filter properties of the device. The fiber-to-fiber gain versus wavelength for a pump power of 200 mW, corresponding to about 80% of the power required to reach lasing threshold, is shown in

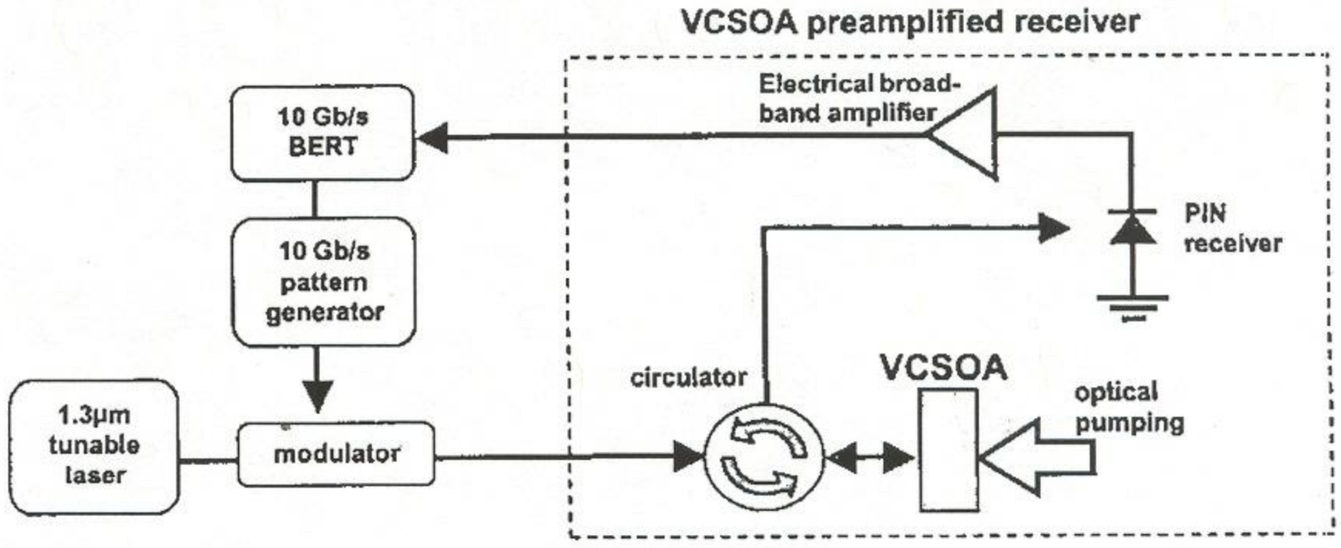

TuW5 Fig. 1. Experimental setup.

Figure 2a. 11 dB fiber-to-fiber gain and an optical bandwidth of 37 GHz (full with half maximum (FWHM)) were measured. The dots correspond to measurements and the line is a curve fit based on the Fabry-Perot equation:

$$G = \frac{(\sqrt{R_t} - \sqrt{R_b}g_s)^2 + 4\sqrt{R_t R_b}g_s \sin^2\varphi}{(1 - \sqrt{R_t R_b}g_s)^2 + 4\sqrt{R_t R_b}g_s \sin^2\varphi} \quad (1)$$

where R_t is top mirror reflectivity, R_b is bottom mirror reflectivity, g_s is gain per pass, and φ is the phase detuning off the cavity resonance wavelength. The measured bandwidth allows for transmission at bit rates up to 33 Gb/s. The isolation of adjacent channels can be determined from the curve fit. At 100 GHz and 50 GHz channel spacing, the suppression of adjacent channels is 14 dB and 8 dB, respectively. Figure 2b shows the bandwidth (FWHM) versus signal gain calculated from Equation 1. The solid line represents the mirror reflectivities of the present device. A decreased pump power results in wider bandwidth, which allows for higher transmission bit rates, but lower signal gain. The maximum obtainable gain as the pump power is increased is in practice limited by the lasing threshold. Higher signal gain and wider gain bandwidth can be simultaneously obtained with lower top mirror reflectivity (curve A). Narrower bandwidth can be obtained with higher mirror reflectivity (curve B) or a longer cavity.

The receiver sensitivity was measured with and without the VCSOA preamplifier. A 10 Gb/s non-return-to-zero $2^{31}-1$ pseudo-random bit sequence was transmitted to the receiver and the bit

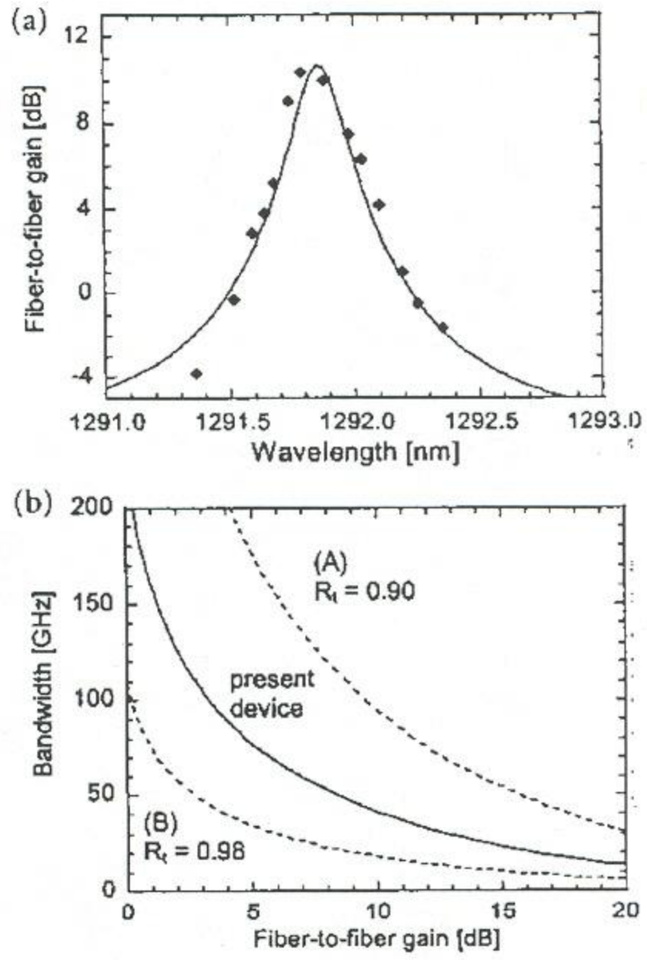

TuW5 Fig. 2. (a) Gain spectrum of VCSOA. (b) Bandwidth (FWHM) vs. signal gain.

error rate (BER) was measured. The BER versus average received optical power is shown in Figure 3. Without the VCSOA, the receiver sensitivity corresponding to a BER of 10^{-9} was –19.2 dBm. With the VCSOA operating at 11 dB fiber-to-fiber

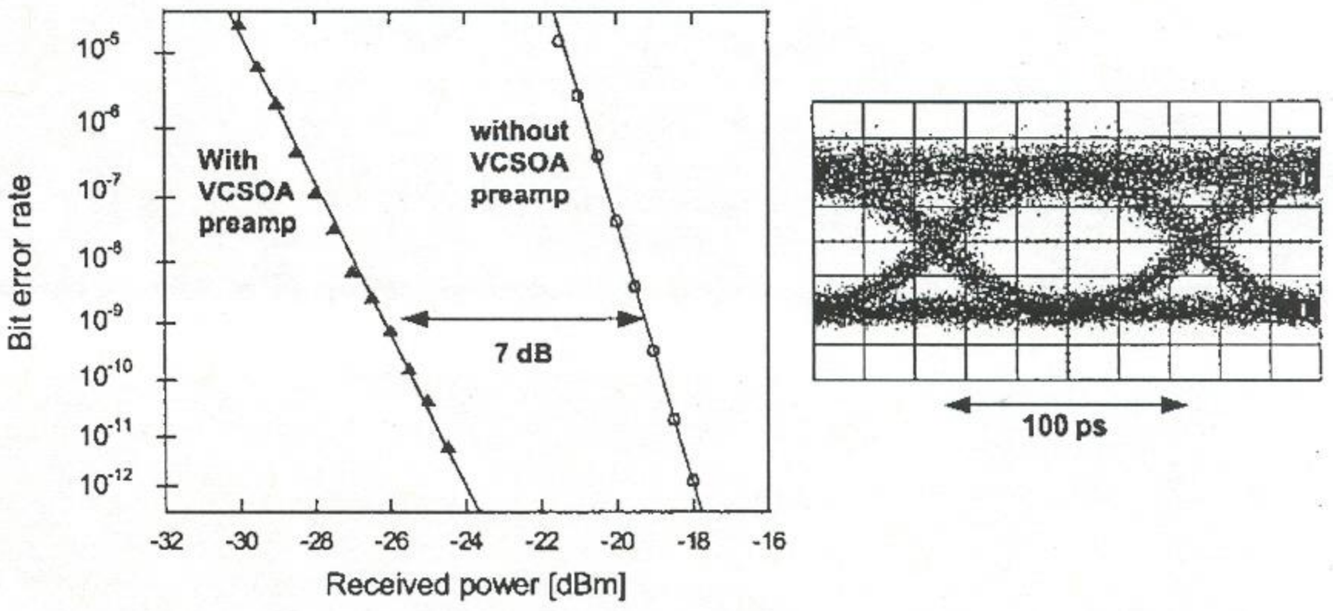

TuW5 Fig. 3. Bit error rate vs. received power and eye diagram for 10 Gb/s transmission.

gain, the receiver sensitivity was improved by 7 dB, resulting in a sensitivity of –26.2 dBm. The 4 dB power penalty is caused by the optical noise added by the VCSOA. No error floor was observed. The eye pattern at a BER of 10^{-9} is also shown in Figure 3. Excess noise from the optical amplification is visible in the high level.

4. Conclusions

We have demonstrated optical preamplification at 10 Gb/s using a VCSOA. The VCSOA has a narrow bandwidth of 37 GHz and functions as an amplifying filter. Operating the VCSOA at 11 dB fiber-fiber gain resulted in a 7 dB improvement in receiver sensitivity. These results suggest that VCSOAs are potential low-cost alternatives to more expensive preamplifiers such as fiber amplifiers. The combined functionality preamplifier-filter is especially attractive for WDM applications where channel selection is needed. Our present device is optimized for reflection mode operation; better isolation of adjacent channels can be obtained using transmission mode operation. Interesting possibilities for future devices include integration of vertical-cavity amplifying filters with photodetectors, either as single devices or 2-dimensional arrays for parallel applications. Tunable receivers could be realized by employing micro electromechanical systems (MEMS), similar to what is being used for tunable VCSELs.[5]

References

1. R.I. Laming, A.H. Gnauck, C.R. Giles, M.N. Zervas, D.N. Payne, "High-Sensitivity Two-Stage Erbium-Doped Fiber Preamplifier at 10 Gb/s," IEEE Photonics Technol. Lett., 4, 1348–1350 (1992).
2. T. Ducellier, R. Basset, J.Y. Emery, F. Pommereau, R. N'Go, J.L. Lafragette, P Aubert, P. Doussière, P. Laube, L. Goldstein, "Record low noise factor (5.2 dB) in 1,55 μm bulk SOA for high bit rate low-noise preamplification," in Tech. Dig. ECOC '96, 3, 173–176 (1996).
3. F. Koyama, S. Kubota, K. Iga, "GaAlAs/GaAs active filter base on vertical cavity surface emitting laser", Electron, Lett., 27, 1093–1095 (1991).
4. A. Black, A.R. Hawkins, N.M. Margalit, D.I. Babic, A.L. Jr. Holmes, Y.-L. Chang, P. Abraham, J.E. Bowers, E.L. Hu, "Wafer fusion: materials issues and device results", IEEE J. Select. Topics Quantum Electron., 3, 943–951, (1997).
5. D. Vakshoori, J.H. Zhou, M. Jiang, M. Azimi, K. McCallion, C.C. Lu, K.J. Knopp, J. Cai, P.D. Wang, P. Tayebati, H. Zhu, P. Chen, "C-band tunable 6 mW vertical-cavity surface emitting lasers", in Technical Digest Optical Fiber Communication Conference (OFC 2000), post-deadline session, PD13 (2000).

TuW6 **5:45 pm**

High-performance 1.55 μm Resonant Cavity Enhanced Photodetector

Ibrahim Kimukin, Necmi Biyikli, Ekmel Ozbay,
Bilkent University, Department of Physics 06533 Ankara, Turkey, Email: kimukin@fen.bilkent.edu.tr

High-performance photodetectors operating at 1.55 μm wavelength are required for ultrafast photodetection in optical communication, measurement, and sampling systems. The photodiode performance is measured by the bandwidth-efficiency product (BWE) and is limited for conventional vertically illuminated photodiodes (VPDs) due to the bandwidth-efficiency tradeoff.[1] This tradeoff arises from the fact that the quantum efficiency and bandwidth of a conventional VPD, have inverse dependencies on the photoabsorption layer thickness. To overcome the BWE limitation for such conventional VPDs, two alternative detection schemes were offered: edge-coupled photodiodes and resonant-cavity-enhanced photodiodes (RCE-PDs). Both PD structures have demonstrated excellent performances and are potential candidates as photodetectors for future high bitrate optical communication systems.[2–6] The ease of fabrication, integration, and optical coupling makes the RCE-PD more attractive for high-performance photodetection.

We used the transfer matrix method to design the epilayer structure and to simulate the optical properties of the photodiode. The bottom Bragg mirror is made of 25 pair quarter-wave stacks (InAlAs/$In_{0.53}Al_{0.13}Ga_{0.34}As$) centered at 1550 nm. The structure was grown by solid-source MBE on semi insulating InP substrate. The details of the epitaxial structure we have used is given in Table 1. The reflectivity measurements showed that the thickness of the epilayers were 3.7% thicker than our design. This shifted the high reflectivity center of the bottom mirror to 1610 nm.

The samples were fabricated by a microwave-compatible process. First ohmic contact to n+ layer was formed by recess etch with a phosphoric acid based etchant that was followed by a self-aligned Au-Ge-Ni liftoff. The p+ ohmic contact was achieved by Ti/Au liftoff. The samples were then rapid thermal annealed at 400°C. Using an isolation mask, we etched away all of the epilayers down to the undoped layer except the active areas. Then we evaporated Ti/Au interconnect metal which formed the coplanar waveguide (CPW) transmission lines on top of the semi-insulating substrate. Silicon nitride layer was deposited using PECVD which is used for both passivation and the insulater layer of metal-insulator-mater capacitors. Finally, a 0.7 mm Au layer was evaporated as an airbridge to connect the center of the CPW to the p+ ohmic metal.

Photoresponse measurements were carried out in the 1530–1630 nm range using a tunable laser source. The output of the laser was coupled to a single mode fiber. The light was delivered to the devices by a lightwave fiber probe, and the electrical characterization was carried out on a microwave probe station. The top p+ layers were

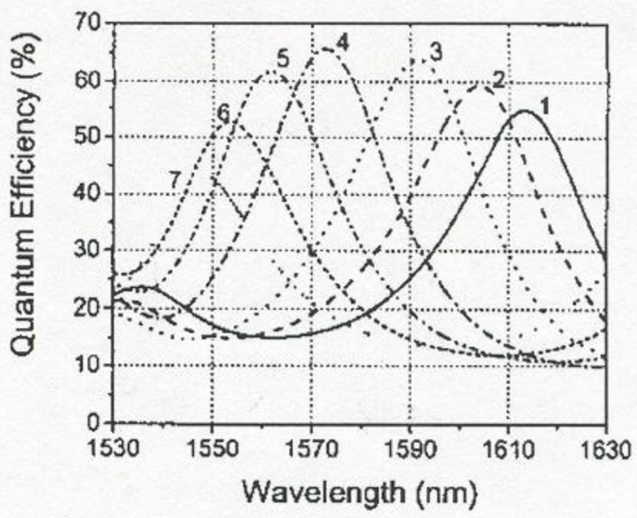

(a)

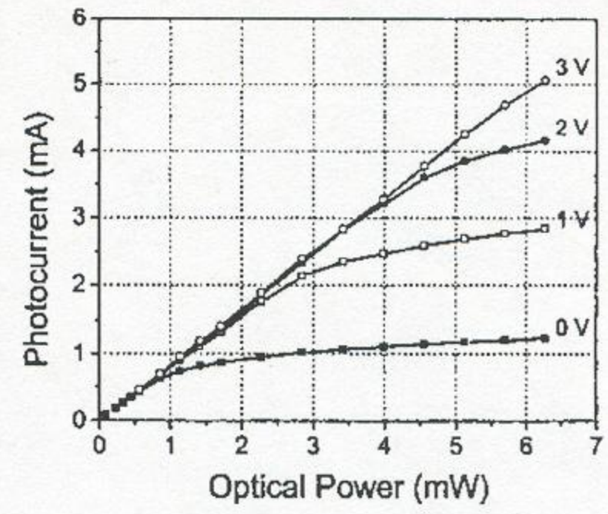

(b)

TuW6 Fig. 1. (a) Spectral quantum efficiency measurements of the fabricated detectors after consecutive recess etches. (b) Optical input power versus photocurrent of the photodetector under various reverse biases.

recess etched in small steps, and the tuning of the resonance wavelength within the high reflectivity spectral region of the DBR was observed.

Fig. 1(a) shows the spectral quantum efficiency measurements of a device under 5 V reverse bias obtained by consecutive ~35 nm recess etches. The peak quantum efficiency increased up to 66% with tuning until the resonance wavelength reached 1572 nm. This increase was due to the increase of the absorption coefficient of InGaAs at shorter wavelengths. As we continued the recess etch, the peak quantum efficiency decreased due to the decrease of the reflectivity of the Bragg mirror. The resonance wavelength was tuned for a total of 47 nm (1538–1605 nm) while keeping the peak efficiencies above 60%. The peak efficiency was above 50% for the resonant

TuW6 Table 1. Epitaxial structure of the wafer

Material	Thickness (nm)	Doping (cm–3)
InGaAs	30	p+ 10^{19}
Graded Layer	30	p+ 10^{19}
InAlAs	210	p+ 10^{19}
InAlAs	50	n– 10^{16}
Graded Layer	30	n– 10^{16}
InGaAs	300	n– 10^{16}
Graded Layer	30	n– 10^{16}
InAlAs	60	n– 10^{16}
InAlAs	300	n+ 3×10^{18}
InAlAs	240	None
25 Pair InAlAs/InAlGaAs DBR	25 × (121/112)	None
InP Substrate	600 μm	Semi-insulating